



Black titania by sonochemistry: A critical evaluation of existing methods

Arno Raes^{a,b}, Rajeshreddy Ninakanti^{a,b}, Lore Van den Bergh^{c,d}, Rituraj Borah^{a,b}, Sabine Van Doorslaer^c, Sammy W. Verbruggen^{a,b,*}

^a Sustainable Energy, Air & Water Technology (DuEL), University of Antwerp, Groenenborgerlaan 171, 2020 Antwerp, Belgium

^b NANOLab Center of Excellence, University of Antwerp, Groenenborgerlaan 171, 2020 Antwerp, Belgium

^c Laboratory of Physics and BioMedical Physics (BIMEF), University of Antwerp, B-2610 Wilrijk, Belgium

^d Laboratory of Adsorption and Catalysis (LADCA), University of Antwerp, B-2610 Wilrijk, Belgium

ARTICLE INFO

Keywords:

Sonochemistry
Ultrasonic synthesis
Titanium dioxide (TiO₂)
Black titania
Lattice defects
Ti³⁺ centres
Oxygen vacancies
Photocatalysis

ABSTRACT

In the field of photocatalysis, the fabrication of black titania is a booming topic, as it offers a system with improved solar light harvesting properties and increased overall efficiency. The darkening of white TiO₂ powders can be ascribed to surface hydroxylation, oxygen vacancies, Ti³⁺ centres, or a combination thereof. A handful of studies suggests these defects can be conveniently introduced by acoustic cavitation, generated during sonochemical treatment of pristine TiO₂ powders. In reproducing these studies, P25 TiO₂ samples were ultrasonicated for various hours with a power density of 8000 W/L, resulting in powders that indeed became gradually darker with increasing sonication time. However, HAADF-STEM revealed that extensive erosion of the sonotrode tip took place and contaminated the samples, which appeared to be the primary reason for the observed colour change. This was confirmed by UV-Vis DRS and DRIFTS, that showed no significant alteration of the catalyst surface after sonication. EPR measurements showed that only an insignificant fraction of Ti³⁺ centres were produced, far less than in a TiO₂ sample that was chemically reduced with NaBH₄. No evidence of the presence oxygen vacancies could be found. The enhanced photocatalytic activities of ultrasonicated materials reported in literature can therefore not be ascribed to the synthesis of actual black (defected) TiO₂, but rather to specific changes in morphology as a result of acoustic cavitation. Also, this study underlines the importance of considering probe erosion in sonochemical catalyst synthesis, which is an unavoidable side effect that can have an important impact on the catalyst appearance, properties and performance.

1. Introduction

Ever since Fujishima and Honda used TiO₂ and UV light to photoelectrocatalytically split water into hydrogen and oxygen in their 1972 landmark study [1], global interest in semiconductor-based photocatalysis has steadily grown. TiO₂ in particular has been investigated extensively for CO₂ conversion [2], water splitting [3,4], and organic pollutant degradation [5,6], due to its chemical and thermal stability, and sustainability [7]. Nevertheless, the catalyst suffers from several inherent shortcomings. Besides its fast charge-carrier recombination rate and limited selectivity, the relatively large band gap (3.0 eV for rutile and 3.2 eV for anatase) allows only for UV light to be absorbed, leaving approximately 95% of the solar spectrum un-utilized by TiO₂ photocatalysis [8,9].

Extending the absorption edge of TiO₂ into the visible region was therefore a logical step towards achieving a more sunlight-responsive

catalyst. In early studies, both metal- and non-metal doping were exploited to obtain a vast array of differently coloured TiO₂ materials, but these were often plagued by lowered crystallinity and higher charge-carrier recombination rates [10,11]. Roughly a decade ago, the interest in coloured TiO₂ surged when Chen *et al.* demonstrated the fabrication of black TiO₂ by hydrogenating TiO₂ nanocrystals under high pressure at elevated temperature, resulting in a material with a band gap extending well into the near-infrared region (1.54 eV), and displaying substantial photocatalytic activity [12]. Following this study, many alternative strategies to synthesise dopant-free coloured or black TiO₂ were explored extensively, resulting in a wide range of different materials with varying properties and characteristics, with often slower recombination rates and increased photocatalytic activities [11,13–16]. Typically, the cause for this colouration effect is attributed to the introduction of lattice disorder, such as Ti³⁺ centres, oxygen vacancies (V_O), surface hydroxylation, and surface hydrogenation, or

* Corresponding author at: Sustainable Energy, Air & Water Technology (DuEL), University of Antwerp, Groenenborgerlaan 171, 2020 Antwerp, Belgium.

E-mail address: Sammy.Verbruggen@uantwerpen.be (S.W. Verbruggen).

<https://doi.org/10.1016/j.ultsonch.2023.106601>

Received 21 June 2023; Received in revised form 31 August 2023; Accepted 13 September 2023

Available online 15 September 2023

1350-4177/© 2023 The Authors. Published by Elsevier B.V. This is an open access article under the CC BY-NC-ND license (<http://creativecommons.org/licenses/by-nc-nd/4.0/>).

combinations thereof.

Because of the time- and energy-intensive nature of most existing synthesis methods, ultrasonic treatment offers a more cost-effective alternative for creating the extreme conditions required to synthesize black TiO₂. The process of acoustic cavitation provides a unique chemical and physical environment, with its hot spots creating local temperatures of up to 5000 K and pressures of up to 500 bar, and allowing for exceptionally high heating and cooling rates (>10⁹ °C s⁻¹) [17]. While this phenomenon has been exploited to synthesize mesoporous and highly crystalline TiO₂ structures through sol-gel methods before [18,19], recent studies propose that acoustic cavitation can be used to induce defects in the TiO₂ lattice, effectively yielding black TiO₂. Fan *et al.* ultrasonically treated amorphous TiO₂ suspensions with a nominal power density of 15,000 W/L, and reported a higher degree of surface hydroxylation with prolonged ultrasonication times [20]. Samples turned darker with longer sonication times, which was attributed to higher hydroxyl concentrations, as no Ti³⁺ or V_O were observed. In their later work, similar conclusions were drawn by ultrasonically treating P25 TiO₂ and other semiconductor nanocrystals in an identical manner: optical absorption increased in the visible and near-infrared regions, which alongside a narrower band gap and enhanced band bending resulted in more darkly coloured materials [21,22]. In addition, altering the pH was shown to have an impact on both the photocatalytic activity of the samples, as on their colour. More alkaline conditions led to a darker grey colour, while also improving the photocatalytic activity. Elavarasan *et al.* reported similar findings after irradiating P25 with an ultrasonic power density of 1000 W/L for several hours at an adjusted pH of 11, but in addition to the surface hydroxylation, they also observed an increase in interplanar distance of the anatase (101) plane with longer sonication times, which they explained by having an increased concentration of V_O in the lattice [23]. Osorio-Vargas *et al.* on the other hand treated P25 for 6 h with a power density of 1200 W L⁻¹ at neutral pH, and partly ascribed the increased visible light absorption of their ultrasonically treated P25 TiO₂ to V_O species generated by the shockwaves and energetic interparticle collisions resulting from the acoustic cavitation [24].

A crucial aspect of sonochemical experiments overlooked in each of these publications, is the so called “reproducibility problem” [25–27]. The power output displayed by the ultrasonic probe device is not necessarily a reflection of the energy delivered to the sonicated medium. Transmission of ultrasonic energy is commonly accompanied by other energetic transformations, such as thermal losses, ultrasonic degassing, breaking of aggregates, or chemical reactions induced by radical formation. In addition, the efficiency of the conversion of electrical energy to acoustic energy is highly dependent on various experimental parameters such as sample volume, tip immersion depth, vessel geometry, tip shape and size, use of cooling bath, *etc.* [28]. Hence, reporting the nominal power output is inaccurate, and will often yield a gross overestimation of the actual acoustic energy transmitted to the sonicated medium. Reporting the actual transmitted energy is therefore essential to be able to reproduce these literature protocols. As of yet, no standardized method of reporting experimental parameters exists, but a straightforward and easily applicable method is the calorimetric method. Such methods have been proposed before by Taurozzi *et al.* [28], and Koda *et al.* [29], for probe sonication and cup horn sonication experiments, respectively, and they only require a thermocouple in order to monitor the temperature change of the sonicated solution over time. By subsequently plotting the measured temperature as a function of time at certain instrument settings, the actual transmitted energy can be approximated by equation (1):

$$P = \frac{dT}{dt} C_p m \quad (1)$$

where P is the transmitted acoustic power, T the temperature, t the time, C_p the specific heat capacity of the medium, and m the mass of the

sonicated volume.

In the context of black TiO₂ synthesis using ultrasonic probes, a second side-effect that is easily overlooked, and perhaps even more important than the previous one, is probe erosion, or pitting erosion. Asymmetric implosion of the cavitation bubbles near the probe tip surface will unavoidably result in microjetting. These are high-velocity liquid streams that are induced by the local high-pressure regions of a collapsing bubble, and will gradually chip away at the probe surface, releasing microscopic metallic probe particles in the sonicated medium, thus potentially darkening the samples. The rate and extent of erosion depends on multiple factors like sonication intensity, time, and frequency, but also on the chemical environment in which the probe is used. Extensive erosion will be visible on the probe surface by an initial matting that will further evolve into a rough surface with extensive pitting. Such a degraded probe surface will in turn also negatively impact the efficiency of energy transmission [28]. The intense and prolonged sonication employed in the studies listed above, would likely result in rapid and extensive tip degradation.

So, in light of these two apparent shortcomings, the objective of this work is also twofold. Firstly, we propose an altered calibration method. Taurozzi *et al.* proposed to carry out calibration in a 600 mL beaker [28], but considering the high (nominal) power densities used in the existing studies (up to 15,000 W/L reported), this method would not be representative for these experiments. We therefore propose to instead perform the calibration in a glass test tube, so as to achieve adequately high power densities through minimisation of the sample volume and optimization of the probe immersion in the liquid. Secondly, we investigate the validity of the claims that high power density sonication of TiO₂ powders can produce black TiO₂, *i.e.* generate crystal defects in the form of Ti³⁺ centres, V_O, and surface hydroxyls. In addition, we explore the influence of probe erosion on the overall colouration of the sample, providing complementary insights to our study.

2. Materials and methods

2.1. Synthesis of ultrasonicated TiO₂

Sonochemical experiments were performed using a Hielscher UP200Ht ultrasonic homogenizer (200 W, 26 kHz), fitted with a titanium alloy sonotrode (Ø 2 mm, Ti-6Al-4 V, type S26d2). The ultrasonic probe was run in continuous mode at 100% amplitude. Sonication times were varied across experiments, as specified.

For construction of the calibration curves, the method of Taurozzi *et al.* [28] was adapted by changing some of the parameters, in order to reach high power densities, not achievable in larger volumes. The method consisted of filling a 1.5 cm diameter borosilicate test tube with 5 mL of distilled water. The ultrasonic horn was then introduced into the liquid, until the tip surface was removed 1 cm from the bottom of the vessel. A thermocouple was introduced to actively monitor the bulk liquid temperature, by placing it at the same depth and at a separation distance of 1 cm from the probe tip surface. The instrument was operated at 100% amplitude and in continuous operation mode. During the experiment, the bulk temperature was plotted as a function of time, and a simple least squares regression model was used to find the optimal linear fit for the first 30 s of sonication. Finally, the actual transmitted power can be estimated from eq. (1).

Sonochemical synthesis experiments were performed in 20 mL test tubes (15 mm × 120 mm) that were carefully immobilised so that the sonotrode did not touch the glass. The set-up was placed inside an ice bath to allow for heat dissipation and maintaining a constant temperature. For each experiment 20 mg of P25 (Aeroxide TiO₂ P25, Evonik) was suspended in 2 mL of double distilled water, at neutral pH, and the probe was inserted up until 1 cm from the bottom of the vessel, since the optimal transmission of ultrasonic energy with our setup was found to be at this position. The experimentally determined power density was approximately 8000 W L⁻¹ under these conditions, which was highest

achievable with our setup. After sonication, the collected sample was dried in an oven at 60 °C overnight and then ground into a fine powder using pestle and mortar. After each experiment, the tip surface of the sonotrode was carefully polished with abrasive paper to ensure a smooth surface for optimal energy transmission during the next experiment.

2.2. Synthesis of chemically reduced TiO₂

As a benchmark experiment, chemically reduced TiO₂ was prepared by first mixing 6 g of pristine P25 TiO₂ nanopowder (Thermo Fisher Scientific) with 8.54 g of NaBH₄ (VWR) for 20 min. The resulting mixture was divided over two trays and heated in a furnace at 350 °C for 60 min under an argon flow of 20 mL min⁻¹. The sample was subsequently cooled down under argon atmosphere, washed once with 10 mM HCl, three times with deionised water, and twice with acetone, and finally dried at 40 °C for 2 h.

2.3. Characterisation

For electron microscopy analysis the samples were dispersed in ethanol, after which 3 µL of solution was drop-casted onto a copper grid coated with a carbon film. An FEI Tecnai Osiris electron microscope in scanning transmission electron microscopy (STEM) mode was employed together with a high-angle annular dark-field (HAADF) detector at 200 kV to obtain the images of the material at the nanoscale, and a super-X EDX detector system was used for obtaining EDX maps of the elemental composition. Quantification of the EDX maps was done using the Cliff Lorimer method [30].

The surface area of the photocatalysts was determined by nitrogen adsorption-desorption measurements at -196 °C. Data were obtained with a 3P meso 112 analyser. All samples were degassed under vacuum at 200 °C for 16 h prior to the measurement. The surface areas were calculated by the Brunauer – Emmet – Teller (BET) method in the P/P_0 interval 0.05 – 0.035.

Potential changes in crystallinity after ultrasonication were investigated by X-ray diffraction (XRD). A Bruker D8 diffractometer with Cu K α_1 ($\lambda = 0.15406$ nm) radiation operating at 40.0 kV and 25.0 mV was employed. Patterns were measured in the 2θ range 10° – 90°, with a scanning rate of 0.04°/0.5 s.

Diffuse reflectance spectra (DRS) were measured with a Shimadzu UV-2600 double beam UV-Vis spectrophotometer, fitted with a two-detector integrating sphere (ISR-2600Plus). The reflectance was recorded in the 300 – 800 nm range at a resolution of 0.2 nm. BaSO₄ was used as the background.

Diffuse reflectance infrared Fourier transform spectroscopy (DRIFTS) was utilized to probe the sample surface for hydroxyl groups. Spectra were measured on a Nicolet Nexus 6700 FT-IR spectrometer, equipped with a DRIFT cell. For analysis, 8 mg of sample was mixed with 392 mg of dry KBr. The cell was placed under vacuum for 30 min before each measurement in order to mitigate the influence of physisorbed water on the sample.

X-band continuous wave (CW) electron paramagnetic resonance (EPR) measurements of the ultrasonicated TiO₂ samples were performed using a Bruker Elexsys E680 X-/W-band spectrometer, using the X-band microwave (mw) frequency of approximately 9.43 GHz. The spectrometer was equipped with a liquid He cryostat (Oxford Inc.), allowing to operate from room temperature, down to 4 K. The X-band CW-EPR spectrum of the chemically reduced TiO₂ sample was measured with a Bruker Elexsys E580 spectrometer with mw frequency around 9.74 GHz. The spectrometer was equipped with a liquid He cryostat (Oxford Inc.) and Stinger cryocooler (ColdEdge), which allowed to measure spectra at temperatures as low as 4 K. The low temperature EPR spectra were recorded at 10 K with a modulation frequency of 100 kHz, modulation amplitude of 0.5 mT, and microwave power of 1 mW. For the determination of the EPR parameters, simulations were performed with the Matlab toolbox EasySpin [31].

Raman spectra were acquired with a Renishaw Invia Qontor Raman microscope, using a 532 nm excitation laser. Measurements were performed in the Raman shift range of 50 – 1000 cm⁻¹. Total accumulation time for each spectrum was 50 s.

Photoluminescence (PL) measurements were performed using a Shimadzu RF-6000 spectrofluorometer, equipped with a Xe lamp. An excitation wavelength of 330 nm was employed, and emission wavelengths ranged from 360 to 675 nm. For both excitation and emission, the slit width was set to 10 nm.

2.4. Evaluation of the photocatalytic activity

The photocatalytic activity of P25 and the ultrasonicated samples were determined through acetaldehyde oxidation experiments, according to the ISO 22197-2 Fine ceramics (advanced ceramics, advanced technical ceramics) – Test method for air-purification performance of semiconducting photocatalytic materials – Part 2: Removal of acetaldehyde [32]. For each test, 50 mg of sample was dispersed in 1 mL of ethanol, drop casted on a 5 × 10 cm test piece, and dried to air. The reactor setup and measurement protocol were as described in the ISO document.

3. Results and discussion

Fig. 1 displays the calibration curves for the ultrasonic probe operating continuously at 100% amplitude, for both a freshly polished probe and an unpolished probe that had already been running at the same settings for 7 h prior to the calibration. In the first 30 s a linear increase of temperature with time is observed for both conditions, with the temperature rise for the unpolished probe being significantly slower. The actual acoustic power densities, determined by applying equation (1), are listed in Table 1, along with their ratio to the nominal power output. For the polished probe, the calculated value approximated the nominal value reasonably well (88%). The same experiment performed with the deteriorated probe, however, resulted in a large discrepancy, with only 53% of the nominal power being effectively transmitted. This demonstrates the necessity of polishing the surface in order to be able to reach the high power densities as expected from the instrumental

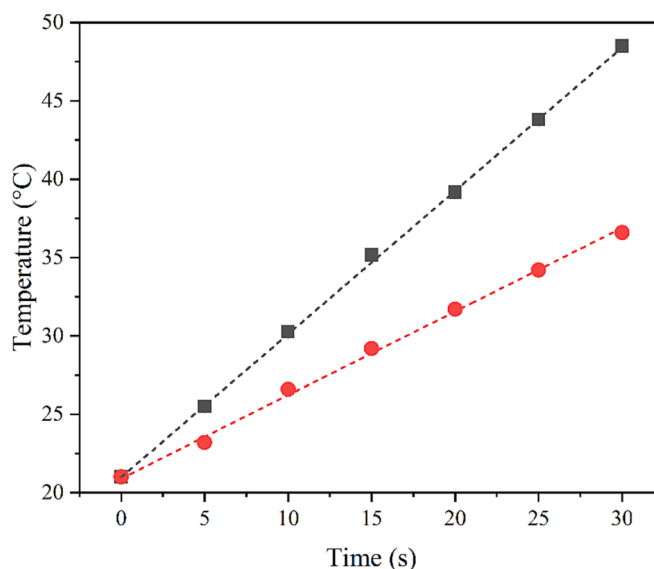


Fig. 1. Calibration curves with linear fit during the first 30 s of sonication. A Hielscher UP200Ht probe fitted with a S26d2 tip was run at 100% amplitude in continuous mode with a polished probe tip (black ■) or an unpolished probe tip after 7 h of preceding operation (red ●). (For interpretation of the references to colour in this figure legend, the reader is referred to the web version of this article.)

Table 1

Comparison of discrepancy between nominal and experimental power densities for experiment with freshly polished probe and degraded probe.

	Nominal P output (W/L)	Experimental P output (W/L)	$P_{\text{exp}}/P_{\text{nom}}$ (%)
Polished probe	4349	3827	88
Unpolished probe	4195	2233	53

settings. Nevertheless, it needs to be considered that polishing the surface too often will shorten the length of the probe and thus change its resonant frequency, making it advisable for the probe to be replaced. Since no such calibrations of the actual transmitted power have been reported in earlier work on sonochemically prepared black TiO₂ [20–24], it is quite possible that the applied power densities were significantly lower than the nominal values listed. For reproducibility purposes it should therefore be stressed that calibrating the actual transmitted power is a crucial parameter to be reported.

Fig. 2 shows P25 exposed to ultrasonic irradiation for different sonication times. Assuming we have an 88% energy transmission efficiency, each sample was treated with a power density of approximately 8000 W/L. The ultrasonic treatment results in powders that become darker with increasing sonication time, going from pristine white to a deep dark grey, as predicted by literature [20–24]. However, when the sonicated suspensions were let to settle overnight first, instead of immediately collecting and drying the powders to obtain samples as in Fig. 2, a dark precipitate was observed to form on the bottom of the vessel (Fig. 3). At the same time, the supernatant regained a colour close to that of the initial suspension prior to sonication. The same observation was made for samples that were sonicated at different power densities and at different pH (Fig. S1). This leads us to believe that the darkening of the sample may not be attributed to the formation of defects due to acoustic cavitation, but rather that erosion fragments were being released from the sonotrode into the suspension, considering the extensive cavitation erosion of the tip that can take place during intense sonication at such high power densities as prescribed by literature. Opto-physical simulations of the colour resulting from such metallic fragments mixed with a white powder, confirm the overall darkened appearance (Supporting Information Fig. S2 and accompanying discussion).

The presence of probe erosion fragments in ultrasonicated P25 was also confirmed experimentally using HAADF-STEM and EDX elemental analysis. As clear from Fig. 4, both large and small, fragmented particles can be observed in the sample, with sizes ranging from several micrometres to a few tens of nanometres. The EDX map proves that these large particles primarily consist of Ti, Al, and V, which are the main components of the titanium alloy probe tip. Elemental quantification of the particles yields atomic percentages of 87.0% Ti, 6.0% Al, and 3.5% V, which is closely aligned with the nominal composition of the Ti-6Al-4V alloy (approximately 90% Ti, 5.5–6.75% Al, and 3.5–4.5% V). Oxygen has a contribution of only 3.5%, meaning little to no TiO₂ is present in these particles, thus confirming that these are not just agglomerates of P25 TiO₂, but in fact solid metallic fragments originating from the

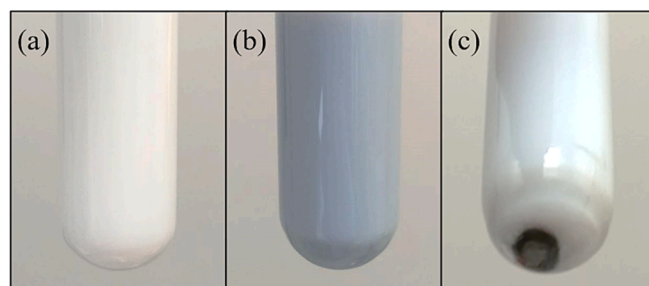


Fig. 3. Suspension of P25 in water (a) before sonication, (b) immediately after 4 h of sonication at 100% amplitude in continuous mode, and (c) after sonication and settling overnight.

ultrasonic probe itself. Furthermore, in the region surrounding these large fragments, atomic percentages of 72.3% and 26.0% are measured for Ti and O, respectively. For pure TiO₂, a Ti to O atomic ratio of 1:2 is expected, instead of the 2.8:1 encountered here. This excessive Ti content thus again results from tip erosion during the sonication process. Combined with the homogeneous distribution of Al (0.7%) and V (1.0%) throughout this region, we can conclude that besides micro-sized erosion, nanoparticulate erosion fragments similar in size to P25 are also generated during sonication, which are homogeneously distributed across the whole sample. Due to the nano- to micron-sized dimensions of these fragments, conventional separation techniques like filtration and centrifugation are typically not sufficiently able to effectively separate these erosion particles from TiO₂ nanoparticles. This was also investigated by Mawson *et al.*, who studied the particle size of ultrasonic probe particulates generated by ultrasonication at higher power densities [33]. While for a 18 kHz operation mode most particulates were removed by a 0.1 μm membrane, small particulates could still be observed even when using a 0.05 μm filter. Therefore, the filtration step performed with a rather coarse 0.22 μm membrane by Osorio-Vargas *et al.* [24] in their procedure for obtaining “black” TiO₂ after ultrasonic treatment, will most likely still result in an erosion-contaminated P25 sample.

The surface areas (S_{BET}) obtained from the N₂ sorption isotherms of P25 and the ultrasonicated P25 samples are listed in Table S1, and show a minor decrease with increasing sonication time, going from 60 m²/g to 52 m²/g. The NaBH₄ reduced P25 sample possesses a slightly smaller surface area (55 m²/g) as well. Average pore volumes (V_{T}) on the other hand increased for the sonicated samples, with volumes up to 0.59 cm³/g compared to 0.31 cm³/g of pristine P25. In contrast, the NaBH₄ reduced sample shows a pore volume of only 0.11 cm³/g.

Fig. 5 presents the XRD patterns of P25, and P25 exposed to ultrasonic irradiation for 1, 4, and 7 h at 100% amplitude. No shifts of diffraction peaks occurred, nor did any peaks disappear, showing that the overall crystalline composition of P25 was maintained well. This is in stark contrast with the XRD pattern of P25 after chemical reduction with NaBH₄, which shows a significantly decreased crystallinity (Fig. S3). The anatase phase can be identified by the following peaks and corresponding crystal planes: 25.3° (101), 37.8° (004), 48.1° (200), and 54.2° (105). For rutile the peaks and corresponding planes are:

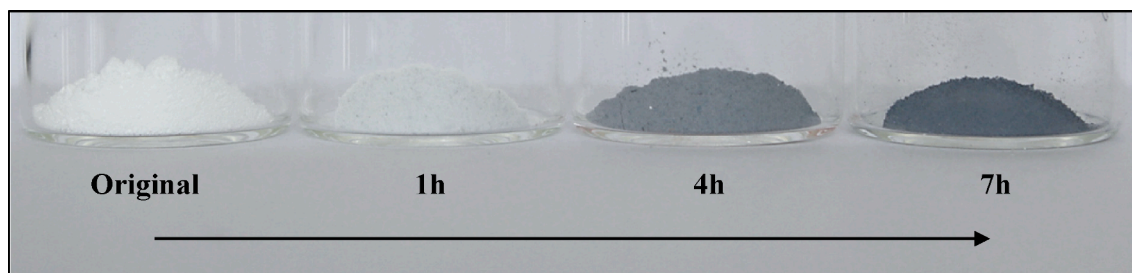


Fig. 2. Colour comparison of pristine P25 and P25 ultrasonicated for different hours at 100% amplitude in continuous mode.

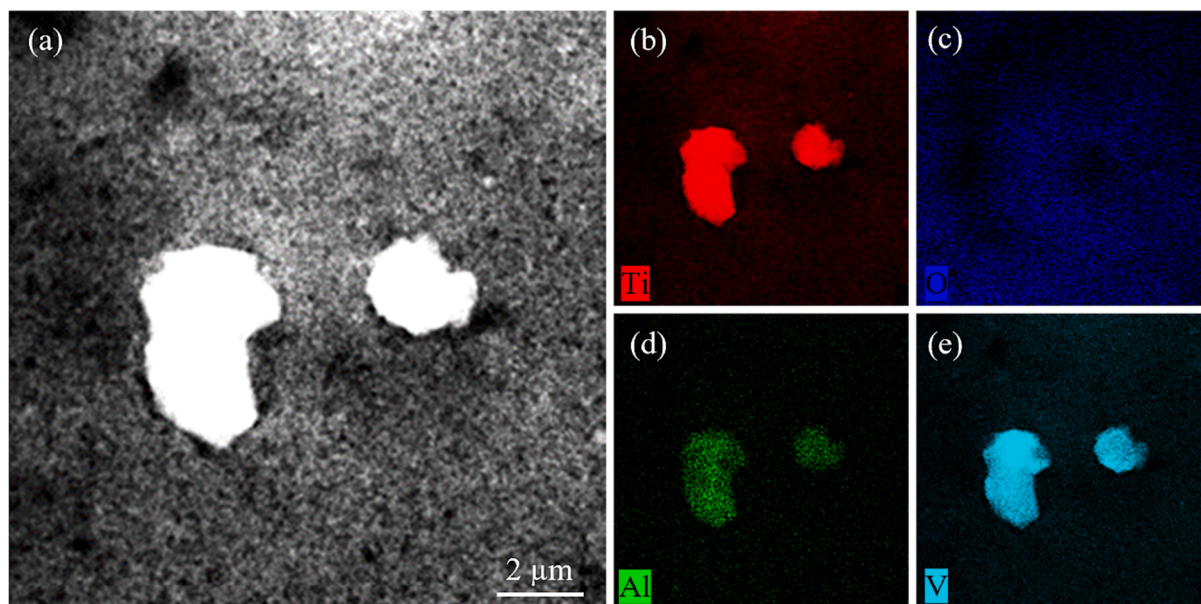


Fig. 4. (a) HAADF-STEM image of P25 TiO₂ with eroded probe tip particles, and EDX mapping of (b) Ti, (c) O, (d) Al, and (e) V.

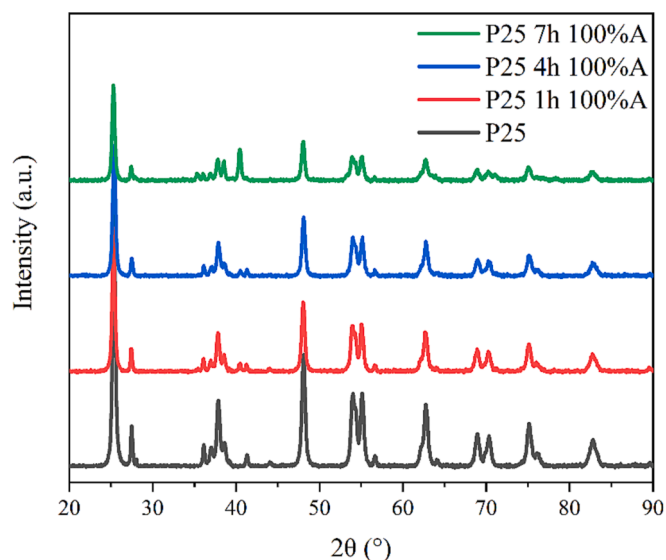


Fig. 5. XRD patterns of pristine P25, and P25 ultrasonically treated for 1, 4, and 7 h at 100% amplitude in continuous mode.

27.4° (110), 36.0° (101), and 42.2° (211) [34]. Notably, a new peak appeared in the diffractogram of the ultrasonicated samples at a 2θ value of 40.6°, which coincides with the expected peak position for metallic Ti [35], arising from the probe erosion. The peak is particularly intense in the sample sonicated for 7 h, demonstrating the extensive probe erosion that can occur in the span of a single experiment. Additionally, the overall peak intensities reduced with increasing sonication time, which could be explained by a potential loss of crystallinity of P25 through the generation of lattice defects, but could also be caused by the erosion particles scattering and absorbing X-rays themselves, thereby lowering the X-ray penetration in the sample, and intensifying the background noise across the entire diffractogram.

Further characterization of the optical properties of these materials was done with UV-Vis DRS, displayed in Fig. 6. As expected from the visual appearance of the samples (Fig. 2), absorption in the visible region increases significantly with increasing ultrasonication time, due to the probe erosion accumulating in the samples during ultrasonic

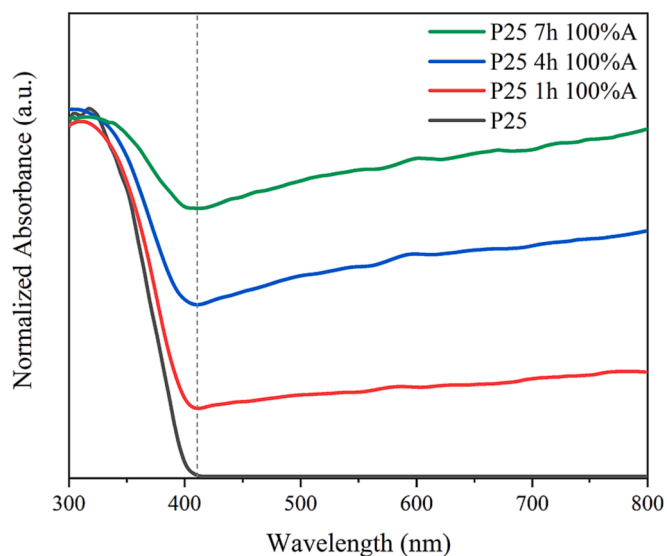


Fig. 6. UV-Vis DR spectra of pristine P25, and P25 ultrasonically treated for 1, 4, and 7 h at 100% amplitude in continuous mode. Vertical dashed line indicates the onset of the absorption edge.

treatment, turning the sample darker. The band edge locations of the ultrasonicated samples are practically identical to that of pristine P25, suggesting no inter-band states were formed, leaving the band gap unaltered. The spectrum of the chemically reduced P25 on the other hand features a substantial blue-shift of the band edge, while also displaying a comparable increase in absorption (Fig. S4). DRIFT spectra of pristine P25 and P25 exposed to ultrasonic irradiation for 1, 4, and 7 h are shown in Fig. 7. All spectra exhibit similar bands, but the curves are shifted towards higher absorbance values with increasing sonication time. Again, this is because of the obviously darker hue of the sonicated P25 samples. None of the samples exhibited any significant changes with respect to the size or shape of the $\nu_{\text{O-H}}$ vibration bands, located in the region $3600 - 3000 \text{ cm}^{-1}$, indicating no or minimal surface modifications were induced by sonication. This contradicts the findings of Fan *et al.* [20,21] and Elavarasan *et al.* [23]. It can be reasoned that increased surface hydroxylation was not necessarily the result of the ultrasonic

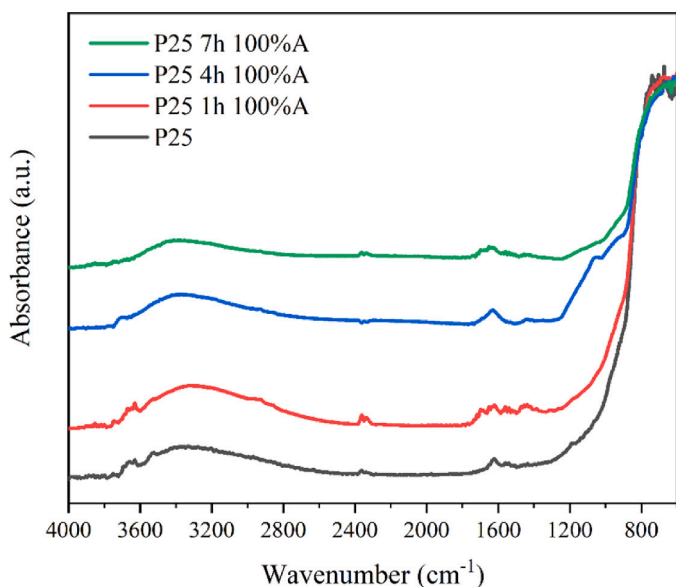


Fig. 7. DRIFT spectra of pristine P25, and P25 ultrasonically treated for 1, 4, and 7 h at 100% amplitude in continuous mode.

treatment, but rather of the alkaline conditions employed in their studies. Noticeable however, is the disappearance of the band around 3695 cm^{-1} , representing isolated chemisorbed OH-groups, which could give an indication of the availability of active sites [36,37].

Since no indications of significantly increased surface hydroxylation were found in our samples, low temperature electron paramagnetic resonance was conducted to survey for bulk and surface defects in the form of O_2^- , Ti^{3+} , or the colour centre V_O (an electron trapped in an oxygen vacancy) and derived species thereof. The results are displayed in Fig. 8. For ultrasound-treated TiO_2 we observe a slightly increased signal intensity ($\times 2.7$) for the resonance at a g -factor of 1.975 (Fig. 8, inset). This signal has been observed before in P25 and ascribed to lattice Ti^{3+} centres in the rutile phase [38]. In addition, sonication induces the formation of a smaller signal with principal g value equal to $[2.0267 \pm$

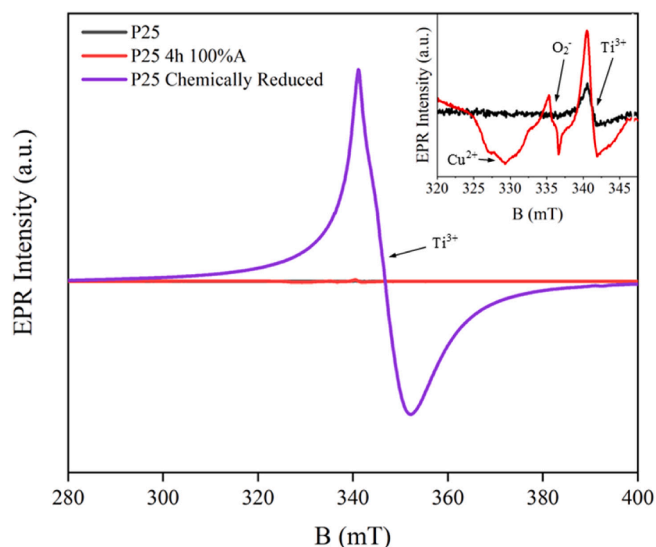


Fig. 8. Comparison of X-band CW-EPR spectra of P25, P25 ultrasonically treated for 4 h at 100% amplitude in continuous mode, and chemically reduced P25. The inset zooms in on the EPR peaks of P25 prior and after ultrasonic treatment. All spectra were measured at 10 K in the presence of air, and are shown normalized to the mass. The spectra are also corrected for the differences in the microwave frequency.

$0.0005\ 2.0084 \pm 0.0003\ 2.0022 \pm 0.0003]$ (Fig. S3). This is due to formation of superoxide radicals (O_2^-) by the reaction of surface Ti^{3+} centres with O_2 to form $\text{Ti}^{4+}-\text{O}_2^-$ [39–41]. We believe Osorio-Vargas *et al.* [24] misinterpreted these EPR signals of ultrasound-treated TiO_2 as O_2^- stabilized on oxygen vacancies. Such superoxide radicals have different principal g values and the sites are far less stable than those stabilized by a titanium surface ion [40]. Furthermore, no evidence of the so-called colour centres (V_O) could be found in the EPR spectra. As a side note, after ultrasonication a signal due to Cu(II) ions is visible in the EPR spectrum of P25. It should be noted that EPR is notoriously sensitive to traces of Cu(II) contamination, that may originate from a spatula or glassware that was used during the synthesis and drying procedure, and even from (distilled) water sources or the cavity of the EPR spectrometer itself, since the probe itself does not contain copper as one of its alloying elements according to its production sheet. Fig. 8 (inset) shows that the overall EPR intensity increases only slightly after the sonication treatment. This contrasts the findings for chemically reduced TiO_2 , which have been reported to induce very strong EPR signals due to the formation of bulk and surface Ti^{3+} centres [41–43]. Fig. 8 illustrates the much larger EPR signal due to Ti^{3+} centres observed upon chemical reduction of P25, here done using NaBH_4 in an argon flow at $350\text{ }^\circ\text{C}$. The peak intensities were normalized based on sample mass, showing that the concentration of Ti^{3+} species and O_2^- in ultrasonicated TiO_2 is negligible compared to that in chemically reduced TiO_2 .

Raman spectra (Fig. S6) are consistent with previous findings. The peak positions remain unchanged, indicating that the vibrational modes associated with the primary crystalline constituents (anatase and rutile) did not undergo substantial changes as a result of ultrasonication. The lower intensity with increasing sonication time may again be mainly attributed to an increased absorption due to the presence of erosion particles. This will lead to a lower amount of incident light reaching the crystal lattice, and thus to a less strong Raman signal.

The PL spectra of P25 and the sonicated samples are displayed in Fig. S7. With longer sonication times, a clear reduction in emission intensity can be observed in both the band centred at 375 nm, and the broad signal in the 385–590 nm range. This less intense signal is likely the result of an enhanced charge carrier separation, stemming from the presence of the erosion particles acting as charge carrier traps. This hypothesis will further be discussed below.

The photocatalytic acetaldehyde oxidation results of the tested materials are presented in Fig. 9. While no evidence of significant alterations to the chemical or structural characteristics of the materials could be found, the photocatalytic activity increases with increasing sonication time, ultimately yielding a near doubling of the photocatalytic activity after ultrasonication for 7 h. These findings are in line with the findings of Fan *et al.* [20], who also reported an increase in activity by a factor 1.97 for their sample with the longest sonication time. Possible explanations for this increase in activity are provided in the paragraphs below.

All of the above findings strongly suggest that ultrasonic synthesis of black TiO_2 is not practically feasible, and that the observed discolouration of white TiO_2 has been misinterpreted in previous research. However, ultrasonic treatment of TiO_2 and other semiconductors can still provide benefits and improve photocatalytic activity significantly, albeit because of other processes associated with acoustic cavitation. Since no significant chemical changes were observed after sonication, morphological changes will most probably play an important role in the enhanced photoactivity. It is known that due to ultrasonic disruption of aggregates and agglomerates, the average particle size of an ultrasonicated sample is often inversely related to the sonication intensity. At the same time, peaking trends have also been reported, where above a certain energy threshold ultrasonication leads to re-agglomeration and sonication-induced aggregate formation [28,44]. Interestingly, both phenomena have been observed for TiO_2 , illustrating the dependence of the surface area on system-specific parameters such as power input and material crystallinity [28]. Moreover, this also demonstrates again the

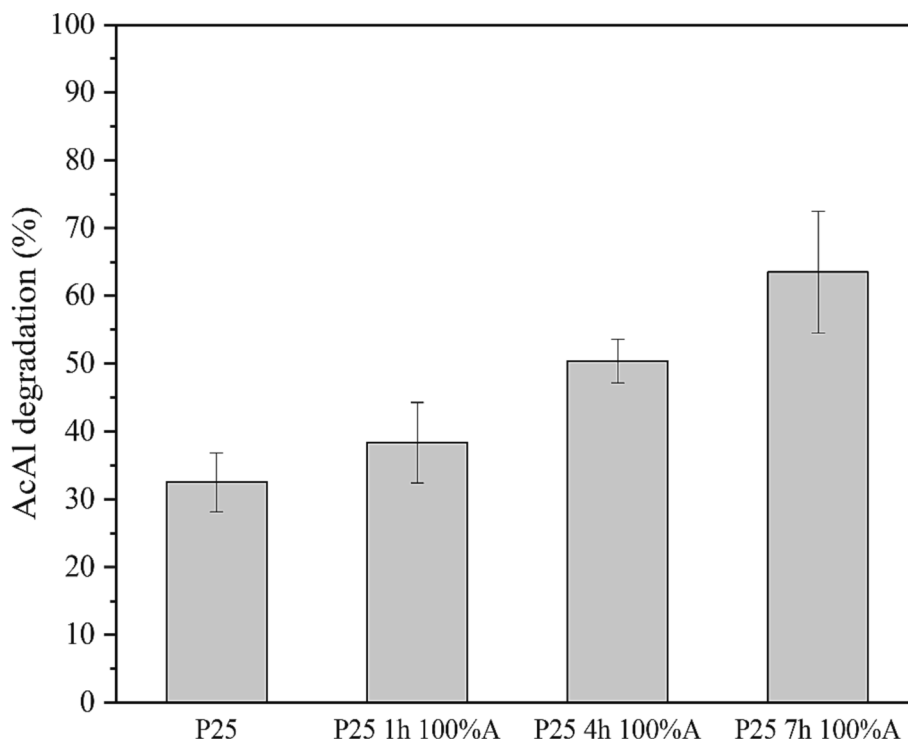


Fig. 9. Photocatalytic activity during an acetaldehyde degradation test. The error bars represent the standard deviation on the measurements.

necessity to have a standardized method for reporting experimental parameters. While we likely suffered from particle aggregation due to a high energy density, Fan *et al.* reported surface areas that doubled after 8 h of ultrasonication [20], which makes for a better distribution of active sites and enhanced accessibility for reactive species. It is therefore likely they achieved a significant increase in active sites available for photocatalysis.

Besides morphological changes, the high-energy conditions resulting from cavitation processes can also induce water sonolysis, which leads to the formation of highly reactive radicals. These radicals can in turn initiate a variety of chemical reactions, including surface modifications like hydroxylation. However, the metallic erosion particles present in our samples may have scavenged these radicals through redox reactions, thus preventing the TiO₂ surface from being hydroxylated. Increasing the available hydroxide ion concentration in the reaction medium by sonicating TiO₂ under alkaline conditions could be a better means to achieve surface hydroxylation. However, although titanium is known to even have an excellent corrosion resistance under alkaline conditions, the combination of the extreme temperatures, pressures, and high alkalinity can lead to an accelerated probe corrosion rate due to the increased reactivity of corrosive hydroxyl species and the higher diffusion rates of ions through the passivated outer layer. Thus, the intended purpose of the alkaline environment may partly be counteracted by faster probe erosion.

Despite the absence of any clear morphological or electronic changes induced by ultrasonication to our samples, the noticeable increase in photocatalytic activity of our samples may be explained by the *in-situ* formation of heterojunctions of TiO₂ and the alloying metals Ti, Al, and V of the ultrasonic probe. Due to the combination of intimate contact between the micron- and nanosized erosion particles with P25, and the highly energetic conditions generated by the ultrasonication, it is expected that metal–semiconductor heterojunctions are formed that could enhance charge separation through formation of a Schottky junction. This could then in turn lead to reduced recombination rates and extended charge carrier lifetimes, which is consistent with the PL results (Fig. S7). While research on TiO₂ junctions with noble metals such as Au, Ag, Pd,

and Pt is plentiful [45], the combination with the metals Ti, Al, and V has received little attention in literature. However, de Brito *et al.* did achieve improved photoactivity by constructing a Ti/TiO₂/CuO n-p junction semiconductor [46].

Another influencing factor might be the presence of chemisorbed dissociated water. As seen in the DRIFT data, the absorption band corresponding to OH-groups chemisorbed on possible active sites became less intense and eventually disappeared upon increasing the sonication time. This might indicate that by ultrasonication terminal OH-groups are effectively removed, increasing the number of available active sites, while not significantly altering the surface area of the material. This would explain the enhanced photocatalytic activity, as the presence of water is known to have a competitive effect on photocatalytic oxidation reactions such as acetaldehyde degradation. Similar observations were made by Carneiro *et al.* [47], Xu *et al.* [48], and recently by Zhang *et al.* [49], who also studied the effect of surface water on the photocatalytic acetaldehyde degradation efficiency. They saw that a weaker interaction between surface water and the TiO₂ surface reduces its competitive behaviour, which eventually leads to an improved acetaldehyde adsorption and degradation capacity.

Lastly, due to the instability of any generated surface defects, or due to the lack thereof in our experiments, only an insignificant amount of lattice defects was formed (O₂ adsorbed on Ti⁴⁺ sites and Ti³⁺). Since no notable changes in surface chemistry were observed, the relatively small amount of lattice disorder was likely caused by thermal and mechanical effects rather than chemical effects. If a certain concentration of TiO₂ is exposed to a microjet or is present in a collapsing bubble, the localized heat and pressure can induce mechanical stress and strain on the TiO₂ lattice. Lattice distortions or rearrangements can be induced by these physical forces, leading to lattice defects. However, we have shown their concentration was negligible in comparison to chemically reduced samples.

4. Conclusion

Critical review of literature on the ultrasonic synthesis of black TiO₂

reinforced the need for an accurate and complete experimental description to accurately reproduce the protocols. Especially calibration of the actual transmitted current density is vital, as it was shown to deviate significantly from the nominal value. Additionally, so far, no attention was given to the influence of probe erosion, which we found to be a dominating phenomenon under the experimental conditions used in literature. While sonication of P25 for prolonged periods of time led to increasingly darker coloured samples, no significant electronic changes were measured. Therefore, the reason for increased optical absorption was not the creation of defects but rather the release of eroded probe fragments into the sonicated suspensions. This makes us assume that literature claims on the synthesis of black TiO₂ through ultrasonication may have been subject to misinterpretation, as the colouration effect of erosion particles is quite prominent.

CRediT authorship contribution statement

Arno Raes: Conceptualization, Methodology, Validation, Formal analysis, Investigation, Writing – original draft, Visualization. **Rajeshreddy Ninakanti:** Validation, Formal analysis, Investigation, Writing – review & editing, Visualization. **Lore Van den Bergh:** Validation, Formal analysis, Investigation, Writing – review & editing, Visualization. **Rituraj Borah:** Validation, Formal analysis, Investigation, Writing – review & editing, Visualization. **Sabine Van Doorslaer:** Conceptualization, Methodology, Resources, Supervision, Writing – review & editing, Funding acquisition. **Sammy W. Verbruggen:** Conceptualization, Methodology, Resources, Writing – review & editing, Supervision, Funding acquisition.

Declaration of Competing Interest

The authors declare that they have no known competing financial interests or personal relationships that could have appeared to influence the work reported in this paper.

Data availability

Data will be made available on request.

Acknowledgements

This work was supported by the University of Antwerp Special Research Fund (BOF-GOA project 41826). We wish to thank Prof. Dr. Vera Meynen for her support and insightful discussions.

Appendix A. Supplementary data

Supplementary data to this article can be found online at <https://doi.org/10.1016/j.ultsonch.2023.106601>.

References

- [1] A. Fujishima, K. Honda, Electrochemical photolysis of water at a semiconductor electrode, *Nature* 238 (1972) 37–38, <https://doi.org/10.1038/238037a0>.
- [2] S.N. Habisreutinger, L. Schmidt-Mende, J.K. Stolarczyk, Photocatalytic reduction of CO₂ on TiO₂ and other semiconductors, *Angew. Chem. Int. Ed.* 52 (29) (2013) 7372–7408.
- [3] J. Tang, J.R. Durrant, D.R. Klug, Mechanism of photocatalytic water splitting in TiO₂. Reaction of water with photoholes, importance of charge carrier dynamics, and evidence for four-hole chemistry, *J. Am. Chem. Soc.* 130 (42) (2008) 13885–13891.
- [4] G.L. Chiarello, M.V. Dozzi, E. Selli, TiO₂-based materials for photocatalytic hydrogen production, *J. Energy Chem.* 26 (2) (2017) 250–258.
- [5] A. Fujishima, X. Zhang, D. Tryk, TiO₂ photocatalysis and related surface phenomena, *Surf. Sci. Rep.* 63 (12) (2008) 515–582.
- [6] D. Chen, Y. Cheng, N. Zhou, P. Chen, Y. Wang, K. Li, S. Huo, P. Cheng, P. Peng, R. Zhang, L.u. Wang, H. Liu, Y. Liu, R. Ruan, Photocatalytic degradation of organic pollutants using TiO₂-based photocatalysts: a review, *J. Clean. Prod.* 268 (2020).
- [7] J. Schneider, M. Matsuoka, M. Takeuchi, J. Zhang, Y. Horiuchi, M. Anpo, D. W. Bahnemann, Understanding TiO₂ photocatalysis: mechanisms and materials, *Chem. Rev.* 114 (2014) 9919–9986.
- [8] M.D. Hernández-Alonso, F. Fresno, S. Suárez, J.M. Coronado, Development of alternative photocatalysts to TiO₂: challenges and opportunities, *Energy Environ. Sci.* 2 (2009) 1231–1257.
- [9] C. Byrne, G. Subramanian, S.C. Pillai, Recent advances in photocatalysis for environmental applications, *J. Environ. Chem. Eng.* 6 (3) (2018) 3531–3555.
- [10] X. Chen, S.S. Mao, Titanium dioxide nanomaterials: synthesis, properties, modifications, and applications, *Chem. Rev.* 107 (2007) 2891–2959.
- [11] T.S. Rajaraman, S.P. Parikh, V.G. Gandhi, Black TiO₂: A review of its properties and conflicting trends, *Chem. Eng. J.* 389 (2020), 123918, <https://doi.org/10.1016/j.cej.2019.123918>.
- [12] X. Chen, L. Liu, P.Y. Yu, S.S. Mao, Increasing solar absorption for photocatalysis with black hydrogenated titanium dioxide nanocrystals, *Science* 331 (6018) (2011) 746–750.
- [13] A. Naldoni, M. Allieta, S. Santangelo, M. Marelli, F. Fabbri, S. Cappelli, C. L. Bianchi, R. Psaro, V. Dal Santo, Effect of nature and location of defects on bandgap narrowing in black TiO₂ nanoparticles, *J. Am. Chem. Soc.* 134 (2012) 7600–7603, <https://doi.org/10.1021/ja3012676>.
- [14] A. Naldoni, C.L. Bianchi, C. Pirola, K.S. Suslick, Porous TiO₂ microspheres with tunable properties for photocatalytic air purification, *Ultrason. Sonochem.* 20 (2013) 445–451, <https://doi.org/10.1016/j.ultsonch.2012.07.003>.
- [15] M. Janczarek, E. Kowalska, Defective dopant-free TiO₂ as an efficient visible light-active photocatalyst, *Catalysts* 11 (8) (2021) 978.
- [16] S.S. Sahoo, S. Mansingh, P. Babu, K. Parida, Black titania an emerging photocatalyst: review highlighting the synthesis techniques and photocatalytic activity for hydrogen generation, *Nanoscale Adv.* 3 (2021) 5487–5524.
- [17] K.S. Suslick, Sonochemistry, *Science* 247 (1990) 1439–1445, <https://doi.org/10.1126/science.247.4949.1439>.
- [18] J. Yu, L. Zhang, J. Yu, Direct sonochemical preparation and characterization of highly active mesoporous TiO, *Chem. Mater.* 14 (2002) 4647–4653, <https://doi.org/10.1021/cm0203924>.
- [19] S.-Y. Kim, T.-S. Chang, C.-H. Shin, Enhancing effects of ultrasound treatment on the preparation of TiO₂ photocatalysts, *Catal. Lett.* 118 (2007) 224–230, <https://doi.org/10.1007/s10562-007-9174-x>.
- [20] C. Fan, C. Chen, J. Wang, X. Fu, Z. Ren, G. Qian, Z. Wang, Black hydroxylated titanium dioxide prepared via ultrasonication with enhanced photocatalytic activity, *Sci. Rep.* 5 (2015) 1–10.
- [21] C. Fan, X. Fu, L. Shi, S. Yu, G. Qian, Z. Wang, Disorder modification and photocatalytic activity enhancement of TiO₂ nanocrystals through ultrasonic hydroxylation, *J. Alloy. Compd.* 703 (2017) 96–102.
- [22] C. Fan, S. Yu, G. Qian, Z. Wang, Ultrasonic-induced disorder engineering on ZnO, ZrO₂, Fe₂O₃ and SnO₂ nanocrystals, *RSC Adv.* 7 (30) (2017) 18785–18792.
- [23] M. Elavarasan, K. Uma, T.C. Yang, Photocatalytic oxidation of ethanol using ultrasonic modified TiO₂; an in-situ diffuse reflectance infrared spectroscopy study, *Results Phys.* 13 (2019), 102237.
- [24] P.A. Osorio-Vargas, C. Pulgarin, A. Sienkiewicz, L.R. Pizzio, M.N. Blanco, R. A. Torres-Palma, C. Pétrier, J.A. Rengifo-Herrera, Low-frequency ultrasound induces oxygen vacancies formation and visible light absorption in TiO₂ P-25 nanoparticles, *Ultrason. Sonochem.* 19 (3) (2012) 383–386.
- [25] T. Mason, Practical Sonochemistry. A Users Guide to Applications in Chemistry and Chemical Engineering, 1991.
- [26] R.F. Contamine, A.M. Wilhelm, J. Berlan, H. Delmas, Power measurement in sonochemistry, *Ultrason. Sonochem.* 2 (1) (1995) S43–S47.
- [27] T. Kimura, T. Sakamoto, J.-M. Leveque, H. Sohmiya, M. Fujita, S. Ikeda, T. Ando, Standardization of ultrasonic power for sonochemical reaction, *Ultrason. Sonochem.* 3 (3) (1996) S157–S161.
- [28] J. Taurozzi, V. Hackley, M. Wiesner, Ultrasonic dispersion of nanoparticles for environmental, health and safety assessment issues and recommendations, *Nanotoxicology* 5 (2010) 711–729, <https://doi.org/10.3109/17435390.2010.528846>.
- [29] S. Koda, T. Kimura, T. Kondo, H. Mitome, A standard method to calibrate sonochemical efficiency of an individual reaction system, *Ultrason. Sonochem.* 10 (2003) 149–156, [https://doi.org/10.1016/S1350-4177\(03\)00084-1](https://doi.org/10.1016/S1350-4177(03)00084-1).
- [30] G. Cliff, G.W. Lorimer, The quantitative analysis of thin specimens, *J. Microsc.* 103 (1975) 203–207, <https://doi.org/10.1111/j.1365-2818.1975.tb03895.x>.
- [31] S. Stoll, A. Schweiger, EasySpin, a comprehensive software package for spectral simulation and analysis in EPR, *J. Magn. Reson.* 178 (1) (2006) 42–55.
- [32] International Standard Organization, ISO 22197-2:2019 Fine Ceramics (Advanced Ceramics, Advanced Technical Ceramics) — Test Method for Air-Purification Performance of Semiconducting Photocatalytic Materials — Part 2, (2019).
- [33] R. Mawson, M. Rout, G. Ripoll, P. Swiergon, T. Singh, K. Knoerzer, P. Juliano, Production of particulates from transducer erosion: Implications on food safety, *Ultrason. Sonochem.* 21 (6) (2014) 2122–2130.
- [34] K. Thamaphat, P. Limsuwan, B. Ngotawornchai, Phase characterization of TiO₂ powder by XRD and TEM, *Agric. Nat. Resour.* 42 (2008) 357–361.
- [35] E. Galvanetto, F.P. Galliano, F. Borgioli, U. Bardì, A. Lavacchi, XRD and XPS study on reactive plasma sprayed titanium–titanium nitride coatings, *Thin Solid Films* 384 (2) (2001) 223–229.
- [36] R. Borah, R. Ninakanti, G. Nuyts, H. Peeters, A. Pedraza-Tardajos, S. Nuti, C. Vande Velde, K. De Wael, S. Lenaerts, S. Bals, S.W. Verbruggen, Selectivity in the ligand functionalization of photocatalytic metal oxide nanoparticles for phase transfer and self-assembly applications, *Chem. – Eur. J.* 27 (2021) 9011–9021, <https://doi.org/10.1002/chem.202100029>.

- [37] M.A. Henderson, An HREELS and TPD study of water on TiO₂(110): the extent of molecular versus dissociative adsorption, *Surf. Sci.* 355 (1996) 151–166, [https://doi.org/10.1016/0039-6028\(95\)01357-1](https://doi.org/10.1016/0039-6028(95)01357-1).
- [38] D.C. Hurum, A.G. Agrios, K.A. Gray, T. Rajh, M.C. Thurnauer, Explaining the enhanced photocatalytic activity of degussa P25 mixed-phase TiO₂ using EPR, *J. Phys. Chem. B* 107 (2003) 4545–4549, <https://doi.org/10.1021/jp0273934>.
- [39] T. Berger, M. Sterrer, O. Diwald, E. Knözinger, D. Panayotov, T.L. Thompson, J. T. Yates, Light-induced charge separation in anatase TiO₂ particles, *J. Phys. Chem. B* 109 (2005) 6061–6068, <https://doi.org/10.1021/jp0404293>.
- [40] J. Green, E. Carter, D.M. Murphy, Interaction of molecular oxygen with oxygen vacancies on reduced TiO₂: site specific blocking by probe molecules, *Chem. Phys. Lett.* 477 (2009) 340–344, <https://doi.org/10.1016/j.cplett.2009.07.002>.
- [41] S. Livraghi, M. Rolando, S. Maurelli, M. Chiesa, M.C. Paganini, E. Giamello, Nature of reduced states in titanium dioxide as monitored by electron paramagnetic resonance. II: Rutile and brookite cases, *J. Phys. Chem. C* 118 (2014) 22141–22148, <https://doi.org/10.1021/jp5070374>.
- [42] S. Livraghi, M. Chiesa, M.C. Paganini, E. Giamello, On the nature of reduced states in titanium dioxide as monitored by electron paramagnetic resonance. I: The anatase case, *J. Phys. Chem. C* 115 (2011) 25413–25421, <https://doi.org/10.1021/jp209075m>.
- [43] A. Naldoni, M. Altomare, G. Zoppellaro, N. Liu, Š. Kment, R. Zboril, P. Schmuki, Photocatalysis with reduced TiO₂: from black TiO₂ to cocatalyst-free hydrogen production, *ACS Catal.* 9 (2019) 345–364, <https://doi.org/10.1021/acscatal.8b04068>.
- [44] D.A. Giannakoudakis, N. Farahmand, D. Łomot, K. Sobczak, T.J. Bandosz, J. C. Colmenares, Ultrasound-activated TiO₂/GO-based bifunctional photoreactive adsorbents for detoxification of chemical warfare agent surrogate vapors, *Chem. Eng. J.* 395 (2020), 125099.
- [45] Y. Wang, T. Wu, Y. Zhou, C. Meng, W. Zhu, L. Liu, TiO₂-based nanoheterostructures for promoting gas sensitivity performance: designs, developments, and prospects, *Sensors* 17 (2017) 1971.
- [46] J.F. de Brito, M.V.B. Zanoni, On the application of Ti/TiO₂/CuO np junction semiconductor: a case study of electrolyte, temperature and potential influence on CO₂ reduction, *Chem. Eng. J.* 318 (2017) 264–271.
- [47] J.T. Carneiro, C.-C. Yang, J.A. Moulijn, G. Mul, The effect of water on the performance of TiO₂ in photocatalytic selective alkane oxidation, *J. Catal.* 277 (2011) 129–133, <https://doi.org/10.1016/j.jcat.2010.10.019>.
- [48] Z. Xu, Y. Ren, X. Deng, M. Xu, W. Chai, X. Qian, Z. Bian, Recent developments on gas-phase volatile organic compounds abatement based on photocatalysis, *Adv. Energy Sustainability Res.* 3 (2022) 2200105, <https://doi.org/10.1002/aesr.202200105>.
- [49] K. Zhang, J. Wang, R. Ninakanti, S.W. Verbruggen, Solvothermal synthesis of mesoporous TiO₂ with tunable surface area, crystal size and surface hydroxylation for efficient photocatalytic acetaldehyde degradation, *Chem. Eng. J.* 474 (2023), 145188, <https://doi.org/10.1016/j.cej.2023.145188>.